INFLUENCE OF TIO_2 SOL-GEL FORMULATION ON MICROSTRUCTURE AND PHOTOCATALYTIC EFFICIENCY OF CERAMIC TILE COATINGS

J.M. Juoi[1]*, M.A. Musa[2], N. Zaharuddin[1] and T.J.S. Anand[3]

[1]Fakulti Teknologi dan Kejuruteraan Industri dan Pembuatan, Universiti Teknikal Malaysia Melaka, Hang Tuah Jaya, 76100 Durian Tunggal, Melaka, Malaysia.

[2]Faculty of Engineering and Technology, Multimedia University, Jalan Ayer Keroh Lama, 75450 Bukit Beruang, Melaka, Malaysia

[3]School of Computing, MIT Vishwaprayag University, Solapur, 413255, India.

*Corresponding Author's Email: jariah@utem.edu.my

Article History: Received 10 March 2025; Revised 20 July 2025; Accepted 16 August 2025

ABSTRACT: The microstructure and crystalline formation of TiO_2 coatings play a decisive role in determining their photocatalytic performance. This study investigates how varying TiO_2 formulations, particularly the incorporation of a commercially available TiO_2 nanopowder (such as Degussa P25), influence the properties of TiO_2 coatings deposited on unglazed ceramic tiles (Ra = 5.50 ± 0.2 μm) via sol–gel dip coating. All coatings were heat-treated at 500 °C, characterized by scanning electron microscope (SEM) and X-ray diffraction (XRD), and evaluated for methylene blue (MB) degradation under ultra-violet (UV) light following ISO 10678:2010. Adding TiO_2 nanopowder markedly modified coating morphology, enabling the formation of continuous, homogeneous nanocomposite layers comprising a TiO_2 matrix binding well-dispersed TiO_2 nanoparticles. This resulted in anatase–rutile phase coexistence, improved adhesion, and reduced cracking, while only modestly increasing overall crystallinity. The TTiP–P25 (50 g/L) formulation exhibited the highest specific photocatalytic activities of $4.74 \times 10^{-5} \pm 1.0 \times 10^{-6}$ for glass slides and $2.99 \times 10^{-5} \pm 1.8 \times 10^{-6}$ for ceramic tiles; surpassing all other formulations. These findings highlight a scalable route to high-performance TiO_2 nanocomposite coatings for durable, self-cleaning building materials.

KEYWORDS: *TiO_2 Nanocomposite; Photocatalysis; Sol–Gel Dip Coating; Ceramic tile*

1.0 INTRODUCTION

Titanium dioxide (TiO_2) has gained considerable attention due to its exceptional photocatalytic activity, chemical stability, and low cost, making it suitable for diverse applications such as self-cleaning surfaces, water purification, air treatment, and antimicrobial coatings [1]. Among the various synthesis techniques, the sol-gel method is one of the most versatile and widely used routes for fabricating TiO_2 thin films and coatings. This process typically involves hydrolysis and condensation of a titanium alkoxide precursor in the presence of solvents and catalysts, followed by gelation, drying, and thermal treatment to form crystalline TiO_2 phases [2].

The sol-gel method offers advantages such as compositional control, ease of doping, and low-temperature processing. It enables the formation of nanostructured TiO_2 coatings on a wide range of substrates, including glass, metals, and ceramics. However, achieving high-quality coatings with optimal photocatalytic activity remains a challenge due to several limitations inherent in the process. Despite its widespread use, sol-gel-derived TiO_2 coatings often suffer from drawbacks such as low crystallinity, small crystal size, high shrinkage upon drying, and the development of cracks due to stress accumulation during thermal treatment [3-6]. Furthermore, coating adhesion and uniformity are often compromised, particularly when deposited on ceramic substrates, leading to poor coating performance [7].

To overcome these limitations, researchers have explored the incorporation of commercial TiO_2 nanoparticles, such as Degussa P25, into sol-gel systems. Degussa P25, a mixed-phase TiO_2 (anatase-rutile) nanopowder, has been widely used due to its superior photocatalytic activity and high surface area [8]. Studies have demonstrated that adding TiO_2 nanopowder to TiO_2 sol-gel precursors can enhance the crystallinity, particle dispersion, and photocatalytic performance of the resulting coatings [9–10] However, these investigations have primarily focused on substrates such as glass and stainless steel, with limited attention given to ceramic materials.

Although significant efforts have been made to improve TiO_2 coating deposition via sol-gel methods, there remains a lack of systematic investigation on the effects of TiO_2 nanopowder addition in TiO_2 sols, particularly for coatings applied to unglazed ceramic tiles. Most previous works have focused on evaluating the final photocatalytic properties of TiO_2 coatings with and without TiO_2 nanopowder addition [11], often neglecting the physicochemical evolution of the sol itself and the intermediate characteristics of the deposited layers. Moreover, the influence of material formulation on coating microstructure, adhesion, and functional performance on ceramic substrates remains underexplored.

This study aims to investigate the effect of incorporating TiO_2 nanopowder into a TiO_2 sol-gel system for the deposition of TiO_2 coatings on unglazed ceramic tiles. Specifically, the objectives are to evaluate the changes in sol characteristics upon TiO_2 nanopowder addition, analyze the morphology, phase composition, and adhesion of the resulting coatings, and assess the photocatalytic performance of the coatings with respect to potential antimicrobial applications. By clarifying the interrelation between sol formulation, coating deposition behavior, and photocatalytic performance, this work contributes to the advancement of sol-gel coating technologies for ceramic substrates. Given the increasing interest in antimicrobial surfaces for public health and environmental applications, the findings from this study could inform the design of more effective TiO_2-based coatings for hygienic ceramic materials. Moreover, understanding the role of TiO_2 nanopowder as an additive may provide a cost-effective strategy to enhance TiO_2 coatings without the need for extensive processing modifications.

2.0 METHODOLOGY

2.1 Preparation of TiO_2 Formulation (TTiP)

Preparation of TiO2 formulation (TTiP) is done via an aqueous sol–gel method through controlled hydrolysis of titanium(IV) isopropoxide (TTiP, 97% purity, Sigma-Aldrich) in a water–ethanol medium (Figure 1). All steps were carried out at ambient temperature inside a fume

hood due to the use of volatile and oxidizing chemicals. The hydrolyzing solution (Solution X) was prepared by adding 8.0 mL of ethanol (95% purity,Polyscientific) to 32.0 mL of deionized water in a reagent bottle, followed by the dropwise addition of 0.40 mL concentrated hydrochloric acid (HCl, 37 % w/w, analytical grade, Merck) using a glass Pasteur pipette while stirring at 500 rpm with a magnetic stirrer. The pH was monitored using a calibrated pH meter and maintained at 1.5 ± 0.1. Separately, the precursor solution (Solution Y) was prepared by mixing 2.0 mL of TTiP with 8.0 mL of ethanol in a 50 mL borosilicate beaker, stirring at 300 rpm for 2 min to ensure homogeneity and slow the subsequent hydrolysis. Solution X was then added to Solution Y dropwise (~1 drop/s) under vigorous stirring at 800 rpm, producing a stable TiO_2 sol (Solution A), which was stirred for an additional 30 min to complete hydrolysis. All glassware was cleaned with ethanol and dried prior to use to avoid contamination.

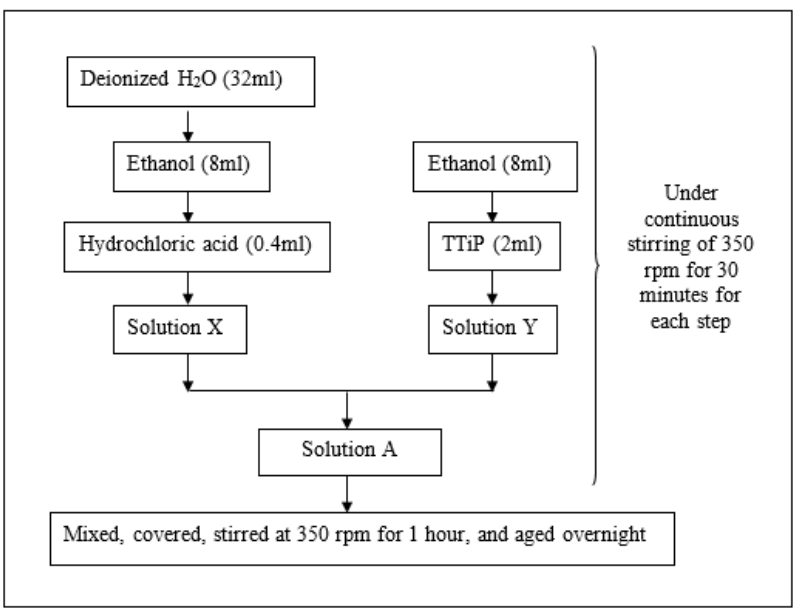

Figure 1: Preparation of TiO2 Formulation Flow Diagram

2.2 Preparation of TiO_2 Nano powder Formulation (P25)

The P25 formulation was prepared using commercial TiO_2 nanoparticles (Degussa P25, Sigma-Aldrich). The process began by adding 16.0 mL of ethanol (95% purity, Polyscientific) to 34.0 mL of deionized water in a reagent bottle. The increased water volume relative to the TiO_2 (TTiP) formulation compensated for the absence of TTiP to maintain total solution volume. The mixture was agitated at 350 rpm for 30 min using a magnetic stirrer before the dropwise addition of 0.40 mL concentrated hydrochloric acid (HCl, 37% w/w, analytical grade, Merck) via a glass Pasteur pipette. Stirring was continued for another 30 min before 2.50 g of Degussa P25 powder was slowly introduced to yield a 50 g/L suspension. The suspension became white and viscous upon nanoparticle dispersion. To minimize agglomeration and ensure homogeneity, the suspension was maintained under continuous stirring at a reduced speed of 180–200 rpm (except during dip-coating) while in storage. All glassware was pre-cleaned with ethanol and oven-dried prior to use to prevent contamination.

2.3 Preparation of TiO_2-TiO_2 Nanopowder Formulation (TTiP-P25)

The TTiP–P25 sol was synthesized using titanium(IV) isopropoxide (TTiP, 97% purity, Sigma-Aldrich) as the TiO_2 precursor and commercial titanium dioxide nanoparticles (Degussa P25, Sigma-Aldrich) as an additive. The TiO_2 sol was first prepared following the procedure described in Section 2.1. Based on previously reported formulations [9, 10] three concentrations of Degussa P25 were identified: 25 g/L, 50 g/L, and 100 g/L, corresponding to 1.25 g, 2.50 g, and 5.00 g of P25 powder, respectively, per 50 mL of TiO_2 sol. The P25 powder was introduced gradually and in small increments to the TiO_2 sol under vigorous stirring at 600–700 rpm using a magnetic stirrer to prevent agglomeration and ensure uniform dispersion. Upon P25 addition, the sol turned white, matching the inherent color of the nanoparticles; higher P25 content yielded progressively thicker and more viscous sols. Following dispersion, each suspension was maintained under continuous stirring for 48 h to facilitate ageing. During storage, the sols were kept under gentle agitation at 180–200

rpm (except during dip-coating) to prevent sedimentation and maintain homogeneity. All glassware was pre-cleaned with ethanol and oven-dried prior to use.

2.3 Dip Coating Deposition

Dip-coating was performed under ambient laboratory conditions using a precision dip-coater (Model DP1000, TEFINI Co., Malaysia; custom-built configuration). For each coating cycle, 25.0 mL of the selected coating formulation; TTiP sol, TTiP–P25 sol, or P25 suspension was placed in a 50 mL borosilicate beaker. The dip-coater was programmed with an immersion and withdrawal speed of 0.5 mm/s and a dwell time of 5 s. During immersion, nanoparticle aggregation, gelation, and partial drying occurred within seconds to minutes, in contrast to bulk sol–gel systems which require days. After each cycle, the coated substrates were suspended vertically using stainless-steel clips and air-dried in a temperature-controlled drying cabinet for 24 h. This was followed by a heat treatment at 110 °C for 30 min in a laboratory oven to ensure complete solvent removal before applying subsequent layers. The procedure was repeated for the desired number of coating cycles, producing films of varying thicknesses corresponding to the number of depositions. All substrates were handled with powder-free nitrile gloves to prevent contamination during processing.

2.4 Characterization

The crystallinity of the coated tiles was characterized using an X-ray diffractometer (PANalytical X'PERT PRO MPD, Model PW 3060/60) equipped with Cu Kα radiation (λ = 1.54060 Å). The instrument was operated at an accelerating voltage of 40 kV and a tube current of 30 mA. Measurements were performed over a 2θ range of 10°–80° using a fixed grazing incidence angle of 4°. Diffraction data were processed and phase identification was conducted using X'Pert HighScore software. The average crystallite size (D) of the anatase and rutile phases was calculated using the Scherrer equation:

$$D = \frac{k\lambda}{\beta \cos \theta} \quad (1)$$

Where, k is a constant (k = 0.94), λ is the X-ray wavelength (0.15406 nm), β is the full width at half maximum of the diffraction peak (in radians), and θ is the Bragg angle. For anatase (A) and rutile (R), the highest-intensity peaks were located at 2θ = 25° (101) and 27° (110), respectively, and these were used for crystallite size determination.

The surface morphology of the Ag–TiO_2 coatings on glazed ceramic tiles was examined using a scanning electron microscope (SEM, JSM-6010PLUS/LV, JEOL Ltd., Japan). Prior to imaging, samples were sputter-coated with a thin gold layer (~10 nm) under an argon atmosphere at 0.05 mbar to enhance conductivity. Elemental composition and distribution were analyzed using energy-dispersive X-ray spectroscopy (EDX) systems integrated with the SEM.

2.3 Photocatalytic

Photocatalytic activity was evaluated following ISO 10678:2010, using methylene blue (MB) degradation as the model reaction. The coated ceramic tiles were first pre-treated by irradiation under a 40 W UV lamp (Philips TUV 40W, Netherlands; λ = 365 nm, intensity ~2.0 mW/cm²) for 24 h to remove surface organic contaminants. Subsequently, each coated tile was immersed in 25.0 mL of aqueous MB solution ($C_{16}H_{18}ClN_3S{\cdot}xH_2O$; analytical grade, Sigma-Aldrich) at an initial concentration of 10 mg/L and kept in the dark for 24 h to establish adsorption–desorption equilibrium. Following conditioning, the coated tiles were placed in fresh 25.0 mL MB solution and exposed to either UV light or visible light from a 200 W halogen lamp for 5 h. During irradiation, the reaction vessels were maintained at ambient temperature (25 ± 2 °C) and continuously stirred at 150 rpm using a magnetic stirrer to ensure homogeneity. Aliquots (3.0 mL) were collected at 1 h intervals, and MB concentration was determined using a UV–Vis spectrophotometer (Shimadzu UV-1700 with a cell length, d of 100mm) by measuring the absorbance at 664 nm. A reference sample, kept in the dark under identical conditions, was analyzed simultaneously to account for photolysis or adsorption effects. The specific degradation rate (R) was calculated using Eq. (2).

$$R = \frac{\Delta A_\lambda \times \nu}{\Delta t \times \varepsilon \times d \times A} \tag{2}$$

Where ΔA_λ is the absorption difference from one measurement to another (1 h to 5 h); V is the volume of MB solution used; Δt is the time

difference; ε is the molar extinction coefficient of MB at 664 nm (ε = 7402.8 m^2/mol); *d* is the measuring cell length used at the spectrophotometer; and *A* is the contact area of MB solution and the catalyst.

The specific degradation rate (R) determined for both irradiated and dark control samples was used to calculate the specific photocatalytic activity (PMB) according to Eq. (3).

$$P_{MB} = R_{irr} - R_{dark} \tag{3}$$

Finally, the photonic efficiency (ζMB) of each sample was determined using Eq. (4), taking into account the photon flux incident on the sample surface and the degradation rate of methylene blue

$$\zeta_{MB} = P_{Mb}/E_P \times 100 \tag{4}$$

Where E_P is the light radiation intensity (W/m^2).

3.0 RESULTS AND DISCUSSION

3.1 Surface morphology

Figure 2 shows SEM images of TiO_2 coatings prepared from three precursors: (i) TTiP-derived sol, (ii) P25 (50 g L^{-1}), and (iii) a TTiP–P25 mixture (50 g L^{-1}). All were deposited on glass and heat-treated at 500 °C for 1 h. The TTiP-derived coating (Figure 2a) displayed pronounced surface non-uniformity, with transparent regions interspersed with opaque deposits caused by gravitational settling during drying. Cracks up to ~5 μm wide indicated poor mechanical integrity and adhesion, conditions known to reduce photocatalytic efficiency by interrupting surface continuity and promoting electron–hole recombination [12].

The P25 coating (Figure 2b) formed a continuous, crack-free film with uniform opacity. Minor agglomerates (2–5 μm) were present, likely from incomplete particle dispersion, but the coating's mesoporous texture and fine pore structure are favorable for photocatalytic activity. These features agree with earlier reports [13–17] of robust, homogeneous P25-based films

produced by dip-coating, spin-coating, and doctor blading. In the other hand, the mixed TTiP–P25 coating (Figure 2c) exhibited a crack-free, sponge-like morphology with irregular particles and a larger, more interconnected pore network than the P25 film. The TTiP sol likely acted as a binder, partially dissolving and redistributing P25 particles to improve cohesion and adhesion. Similar hybrid systems have been shown to combine structural stability with enhanced porosity [18,19]. These findings highlight the strong influence of precursor formulation on coating morphology and potential photocatalytic performance.

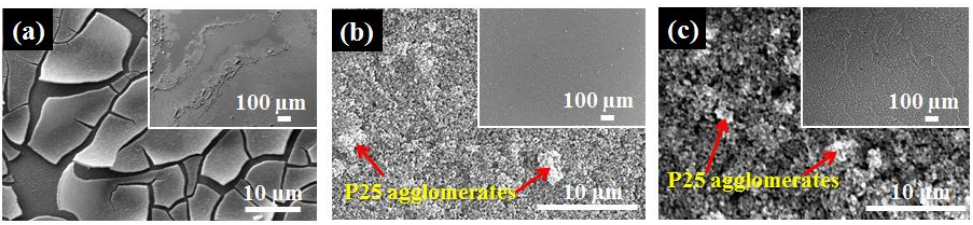

Figure 2: Surface morphology of five dipping TiO_2 coating on glass substrates using different formulation of TiO_2 precursor/ starting materials: (a) TTiP, (b) P25 (50 g/L), and (c) TTiP-P25 (50 g/L). (Insets: morphology at lower magnification – 100x magnifications).

SEM images of TiO_2 coatings deposited on unglazed ceramic tiles using (i) TTiP-derived sol, (ii) P25 (50 g L^{-1}), and (iii) a TTiP–P25 mixture (50 g L^{-1}), after heat treatment at 500 °C for 1 h are shown in Figure 3. The TTiP-only coating (Figure 3a) failed to fully cover the ceramic surface, even after five dipping cycles. Large voids and pores were evident, with only scattered, crumb-like TiO_2 deposits of variable size. This poor surface coverage is attributed to the high porosity and roughness of the ceramic substrate, which absorbed much of the sol, leaving minimal material after drying and calcination.

In contrast, the P25 coating (Figure 3b) formed a dense but inhomogeneous layer, fragmented by macro cracks up to ~30 µm wide. At higher magnification, the typical sponge-like P25 morphology was visible, but adhesion was poor, with flaking and irregular white agglomerates. These defects likely arise from thick film formation, mismatched thermal expansion between coating and substrate, and stresses generated during drying, crystallization, and densification [20,21]. It was also observed that the mixed TTiP–P25 coating (Figure

3c) exhibited a denser, more continuous film with no delamination, though microcracks were present. At higher magnification, the coating showed a smoother sponge-like structure, evenly distributed pores (1–3 μm), and fewer agglomerates, suggesting improved P25 dispersion and reduced stress from the addition of TiO_2 sol. Despite the remaining microcracks, the enhanced coverage, uniformity, and adhesion indicate better functional potential, though long-term stability; particularly under wet conditions remains a consideration [22].

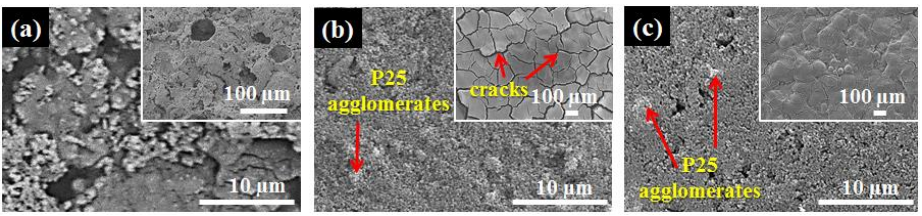

Figure 3: Surface morphology of TiO_2 coating on unglazed ceramic tiles using different formulation (a) TTiP as precursor, (b) P25 (50 g/L), and (c) TTiP-P25 (50 g/L). (Insets: morphology at lower magnification – 100x magnifications).

3.2 Cross section surface

Figure 4 shows cross-sectional SEM images of TiO_2 coatings on unglazed ceramic tiles prepared from (i) P25 (50 g L^{-1}) and (ii) a TTiP–P25 mixture (50 g L^{-1}), after five dipping cycles and calcination at 500 °C for 1 h. The TTiP-only formulation was excluded as no continuous coating formed. It can be seen that the P25 coating (Figure 4a) formed a dense but uneven layer, 30–60 μm thick (average ~38 μm), with visible cracks and a large interfacial void between coating and substrate. Thickness variation reflects the rough, porous ceramic surface, while the absence of a sol–gel binder likely contributed to poor adhesion and crack formation, making the film susceptible to flaking under mechanical stress [23].

In the other hand, the TTiP–P25 coating (Figure 4b) was thinner and more uniform, 10–45 μm thick (average ~29 μm), with fewer cracks and improved substrate adhesion. This enhancement aligns with previous reports [24,25] showing that combining TiO_2 sol with P25 improves cohesion by binding particles into a more stable matrix. The reduced

thickness, smaller cracks, and stronger adhesion are advantageous for photocatalytic performance, providing greater accessible surface area for photon absorption and pollutant interaction while improving mechanical durability.

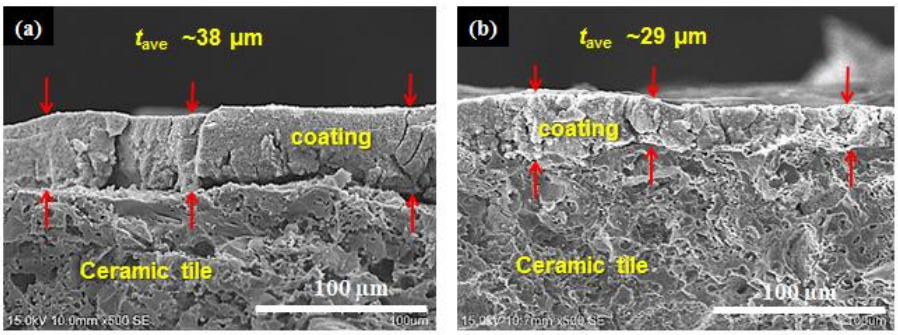

Figure 4: SEM Cross-sectional morphology and average thickness (t_{ave}) of TiO_2 coating deposited on unglazed ceramic tile with different TiO_2 precursor: (a) P25 (50 g/L) only, and (b) TTiP - P25 (50 g/L).

3.3 Crytalline phases

Figure 5 shows GAXRD patterns of TiO_2 coatings prepared from different precursor formulation; TTiP-derived sol, P25 (50 g L^{-1}), and a TTiP–P25 mixture (50 g L^{-1}) after five dipping cycles and calcination at 500 °C for 1 h, on unglazed ceramic tiles (Figure 5a) and glass substrates (Figure 5b). On the unglazed ceramic tiles, the TTiP-only coating shows no obvious TiO_2 diffraction peaks, as strong ceramic substrate peaks obscured any potential signal. This aligns with SEM observations of incomplete coverage. In contrast, the P25 coating exhibits clear anatase (101) and rutile (110) reflections at $2\theta = 25.3°$ and 27.5°, respectively, along with additional anatase and rutile peaks, confirming continuous coverage despite surface cracking. The TTiP-P25 coating produced a similar diffraction pattern to P25 alone, indicating complete substrate coverage and confirming that the sol–gel component filled pores and cracks without altering the crystalline phase composition.

On glass substrates, the TTiP-only coating displayed a weak anatase (101) peak at 25.3°, consistent with typical sol–gel-derived TiO_2 [26]. The P25 coating exhibits stronger anatase and rutile peaks, reflecting the dual-phase nature of P25. The TTiP-P25 coating shows a similar pattern to P25 but with slightly enhanced anatase peak intensity, suggesting synergistic crystallization contributions from both the sol–gel and nanoparticle components.Crystallite size calculations using Scherrer's equation for the anatase (101) peak yielded 5 nm for TTiP, 23 nm for P25, and 22 nm for TTiP–P25. These results indicate that incorporating P25 substantially increased crystallite size and crystallinity compared with TTiP alone, due to the presence of pre-formed anatase and rutile nanoparticles [24]. Here, the data show that formulation strongly influences TiO_2 crystallinity where TTiP alone produces small, weakly crystalline anatase domains; P25 yields a well-defined mixed-phase structures with larger crystallites; and TTiP-P25 mixture maintain P25's crystallinity while enhancing surface coverage and uniformity.

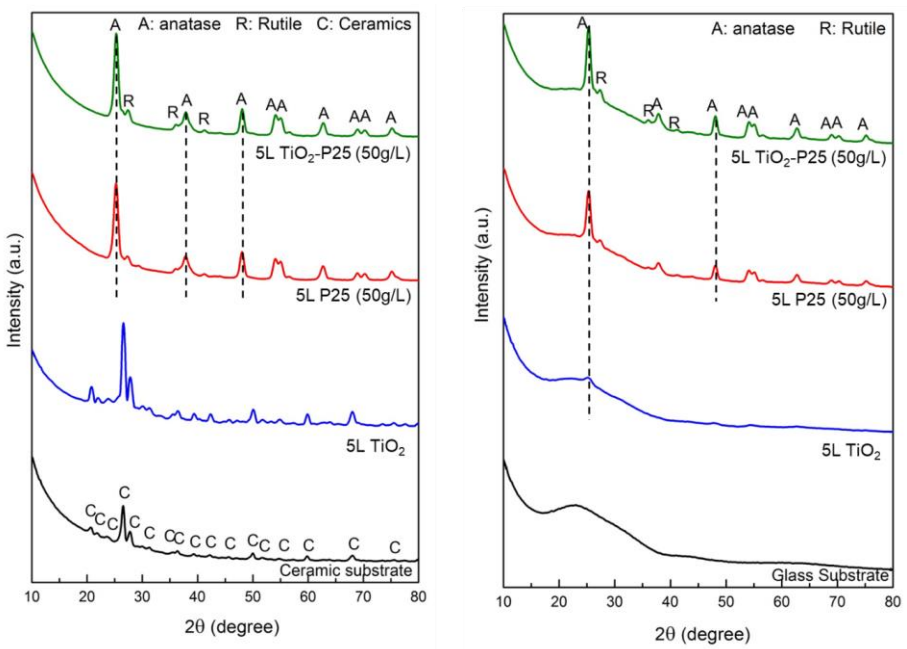

(a) (b)

Figure 5: GAXRD diffractograms of TiO2 coatings using three different TiO2 formulation coated at five dipping times deposited on: (a) unglazed ceramic tiles; (b) glass substrate, after heat treatment at 500°C for one hour.

3.4 Photocatalytic Performances

Table 1 summarizes the specific photocatalytic activity (P_{MB}) and photonic efficiency (ξ_{MB}) of TiO_2 coatings prepared from TTiP-derived sol, P25 (50 g L^{-1}), and a TTiP–P25 mixture (50 g L^{-1}), on glass and unglazed ceramic substrates. In all cases, coatings on glass exhibits higher P_{MB} and ξ_{MB} values than those on ceramic tiles, reflecting the smoother surface and superior film continuity achievable on glass.

Across both substrates, the TTiP–P25 coating showed the highest photocatalytic performance, followed by P25 alone and then TTiP. The superior performance of P25 relative to TTiP is attributable to the presence of well-crystallized TiO_2 nanoparticles in an ~80% anatase to 20% rutile ratio [27], which promotes electron–hole separation and enhances photocatalytic efficiency [28]. SEM and GAXRD analyses confirmed that P25 formed continuous coatings on ceramic tiles, whereas TTiP failed to fully cover the substrate, limiting active surface area. As noted by Petrovic et al. [23], greater photocatalyst coverage directly improves degradation rates by increasing both photon absorption and pollutant adsorption [29].

The incorporation of P25 into the TiO_2 sol further improved performance, consistent with literature reports [22,26]. On glass, P_{MB} values increased from 3.47×10^{-5} for TTiP to 4.74×10^{-5} for TTiP-P25. Comparable increased were observed on ceramic substrates. The enhanced activity of the hybrid formulation can be linked to its distinctive sponge-like morphology, with large open pores that increase exposure of P25 crystallites and facilitate contaminant transport to active sites, as suggested by Chen and Dionysiou [22]. Based on the findings, it can be deduced that formulation plays a critical role related to the photocatalytic performance of the deposited coating, TTiP alone produces low-activity films due to poor coverage and low crystallinity, P25 delivers strong performance through its optimized phase composition and crystallinity, and TTiP–P25 mixtures combine these strengths with improved surface structure, leading to the highest activity on both substrate types.

Table 1: Specific photocatalytic activity, photonic efficiency for TiO_2 coated glass slides and ceramic tiles using different formulation of TiO_2 coatings

Substrate	Type of TiO_2 Precursor	Specific Photocatalytic Activity, P_{MB} (mol/m²h × 10^{-5})	Photonic Efficiency, ξ_{MB} (%)
Glass slides	TTiP	3.47 ± 0.17	1.95E-05
	P25 (50g/L)	3.63 ± 0.52	2.04E-05
	TTiP-P25 (50g/L)	4.74 ± 0.10	2.66E-05
Unglazed Ceramic Tiles	TTiP	2.33 ± 0.60	1.25E-05
	P25 (50g/L)	2.72 ± 0.21	1.46E-05
	TTiP-P25(50g/L)	2.99 ± 0.18	1.60E-05

4.0 CONCLUSION

This work establishes that TiO_2–P25 nanocomposite coatings, prepared via multiple sol–gel dipping cycles, achieve superior structural integrity and photocatalytic performance compared to pure TiO_2. The optimized TTiP–P25 (50 g/L) formulation produced a continuous, homogeneous layer in which the TiO_2 matrix bound the coating while nano TiO_2 particles (P25) acted as functional fillers during crystallization. This interaction delivered the highest photocatalytic activity and methylene blue degradation, demonstrating the coating's strong self-cleaning potential. The findings highlight a novel, scalable approach for integrating high-performance photocatalytic coatings into building materials, paving the way for durable, energy-efficient architectural surfaces.

ACKNOWLEDGMENTS

This work was supported by the Universiti Teknikal Malaysia Melaka through Grant FRGS F00215

AUTHOR CONTRIBUTIONS

J.M. Juoi: Conceptualization, Supervision, Methodology, Writing-Reviewing and editing; M.A.Musa: Data Analysis, Experimental; N. Zaharuddin: Draft Preparation; T. J.S. Anand: Reviewing.

CONFLICTS OF INTEREST

The manuscript has not been published elsewhere and is not under consideration by other journals. All authors have approved the review, agree with its submission and declare no conflict of interest on the manuscript.

REFERENCES

[1] Y. Wei, Q. Wu, H. Meng, Y. Zhang and C. Cao, "Recent advances in photocatalytic self-cleaning performances of TiO_2-based building materials," *RSC Advances*, vol. 13, no. 30, pp. 20584–20597, 2023.

[2] C. K. C. Kayser, L. T. Mueller, L. G. Soares, D. R. Volz, A. L. Ziulkoski, E. L. Schneider, C. T. Oliveira, F. D. P. Morisso, S. R. Kunst and C. L. P. Carone, "Organic-inorganic films with anticorrosive and bactericidal properties for titanium implants," *Materials Research*, vol. 26, art. no. e20230218, 2023.

[3] M. Keshmiri, M. Mohseni and T. Troczynski, "Development of novel TiO_2 sol–gel derived composite and its photocatalytic activities for trichloroethylene oxidation," *Applied Catalysis B: Environmental*, vol. 53, no. 4, pp. 209–219, 2004.

[4] M. Bockmeyer and P. Löbmann, "Crack formation in TiO_2 films prepared by sol–gel processing: quantification and characterization," *Thin Solid Films*, vol. 515, no. 13, pp. 5212–5219, 2007.

[5] X. Guo, L. Rao, P. Wang, C. Wang, Y. Ao, T. Jiang and W. Wang, "Photocatalytic properties of P25-doped TiO_2 composite film synthesized via sol–gel method on cement substrate," *Journal of Environmental Sciences*, vol. 66, pp. 71–80, 2018.

[6] M. Velashjerdi, M. Soleymani and M. Z. Mehrizi, "Preparation of crack-free TiO_2 coating by active screen plasma annealing method," *Materials Today Communications*, vol. 25, art. no. 101316, 2020.

[7] Y. Zhang, X. Zhao, H. Wang, S. Fu, X. Lv, Q. He, R. Liu, F. Ji and X. Xu, "Effect of temperature on the adhesion and bactericidal activities of Ag^+-doped $BiVO_4$ ceramic tiles," *Inorganics*, vol. 10, no. 5, art. no. 61, 2022.

[8] M. El Mchaouri, S. Mallah, D. Abouhajjoub, W. Boumya, R.

Elmoubarki, A. Essadki, N. Barka and A. Elhalil, "Engineering TiO_2 photocatalysts for enhanced visible-light activity in wastewater treatment applications," *Tetrahedron Green Chemistry*, vol. 6, art. no. 100084, 2025.

[9] Y. Chen and D. D. Dionysiou, "TiO_2 photocatalytic films on stainless steel: the role of Degussa P-25 in modified sol–gel methods," *Applied Catalysis B: Environmental*, vol. 62, no. 3–4, pp. 255–264, 2006.

[10] G. Balasubramanian, D. D. Dionysiou, M. T. Suidan, I. Baudin and J. M. Laîne, "Evaluating the activities of immobilized TiO_2 powder films for the photocatalytic degradation of organic contaminants in water," *Applied Catalysis B: Environmental*, vol. 47, no. 2, pp. 73–84, 2004.

[11] C. Chang, S. Rad, L. Gan, Z. Li, J. Dai and A. Shahab, "Review of the sol-gel method in preparing nano TiO_2 for advanced oxidation process," *Nanotechnology Reviews*, vol. 12, no. 1, art. no. 20230150, 2023.

[12] W. T. Soon, A. R. Bushroa and M. Z. Ibrahim, "Effects of Sc_2O_3/ZrO_2 co-doped TiO_2 composite thin layer on the performance of antifogging properties for optical applications," *Journal of the Indian Chemical Society*, vol. 102, no. 9, art. no. 101983, 2025.

[13] I. M. Arabatzis, S. Antonaraki, T. Stergiopoulos, A. Hiskia, E. Papaconstantinou, M. C. Bernard and P. Falaras, "Preparation, characterization and photocatalytic activity of nanocrystalline thin film TiO_2 catalysts towards 3,5-dichlorophenol degradation," *Journal of Photochemistry and Photobiology A: Chemistry*, vol. 149, pp. 237–245, 2002.

[14] D. S. Kim and S. Y. Kwak, "Photocatalytic inactivation of E. coli with a mesoporous TiO_2 coated film using the film adhesion method," *Environmental Science & Technology*, vol. 43, no. 1, pp. 148–151, 2009.

[15] M. Zlámal, J. Krýsa and J. Jirkovský, "Photocatalytic degradation of Acid Orange 7 on TiO_2 films prepared from various powder catalysts," *Catalysis Letters*, vol. 133, no. 1, pp. 160–166, 2009.

[16] G. Kenanakis and N. Katsarakis, "Chemically grown TiO_2 on glass with superior photocatalytic properties," *Journal of Environmental Chemical Engineering*, vol. 2, no. 3, pp. 1748–1755, 2014.

[17] M. Pourmoalem and S. Naghibi, "Potency of commercial TiO_2-P25 nanoparticles to form stainless steel protective coating," *International Journal of Applied Ceramic Technology*, vol. 14, no. 3, pp. 433–442, 2017.

[18] C. Díaz-Uribe, J. Viloria, L. Cervantes, W. Vallejo, K. Navarro, E. Romero and C. Quiñones, "Photocatalytic activity of Ag-TiO_2

composites deposited by photoreduction under UV irradiation," *International Journal of Photoenergy*, vol. 2018, art. no. 7496907, 2018.

[19] Y. Chen and D. D. Dionysiou, "A comparative study on physicochemical properties and photocatalytic behavior of macroporous TiO_2-P25 composite films and macroporous TiO_2 films coated on stainless steel substrate," *Applied Catalysis A: General*, vol. 317, no. 1, pp. 129–137, 2007.

[20] M. Hasmaliza, H. S. Foo and K. Mohd, "Anatase as antibacterial material in ceramic tiles," *Procedia Chemistry*, vol. 19, pp. 828–834, 2016.

[21] A. L. da Silva, M. Dondi and D. Hotza, "Self-cleaning ceramic tiles coated with Nb_2O_5-doped TiO_2 nanoparticles," *Ceramics International*, vol. 43, no. 15, pp. 11986–11991, 2017.

[22] Y. Chen and D. D. Dionysiou, "Effect of calcination temperature on the photocatalytic activity and adhesion of TiO_2 films prepared by the P-25 powder-modified sol–gel method," *Journal of Molecular Catalysis A: Chemical*, vol. 244, no. 1–2, pp. 73–82, 2006.

[23] V. Petrovič, V. Ducman and S. D. Škapin, "Determination of the photocatalytic efficiency of TiO_2 coatings on ceramic tiles by monitoring the photodegradation of organic dyes," *Ceramics International*, vol. 38, no. 2, pp. 1611–1616, 2012.

[24] Y. Sun and K. Yan, "Sol-gel modified TiO_2 powder composite films for photoelectrochemical hydrogen generation," *Journal of Advanced Oxidation Technologies*, vol. 19, no. 2, pp. 376–380, 2016.

[25] K. M. Tarquinio, N. K. Kothurkar, D. Y. Goswami, R. C. Sanders Jr., A. L. Zaritsky and A. M. LeVine, "Bactericidal effects of silver plus titanium dioxide-coated endotracheal tubes on Pseudomonas aeruginosa and Staphylococcus aureus," *International Journal of Nanomedicine*, vol. 5, pp. 177–183, 2010.

[26] F. Oshani, R. Marandi, S. Rasouli and M. K. Farhoud, "Photocatalytic investigations of TiO_2–P25 nanocomposite thin films prepared by peroxotitanic acid modified sol–gel method," *Applied Surface Science*, vol. 311, pp. 308–313, 2014.

[27] J. He, Y. E. Du, Y. Bai, J. An, X. Cai, Y. Chen, P. Wang, X. Yang and Q. Feng, "Facile formation of anatase/rutile TiO_2 nanocomposites with enhanced photocatalytic activity," *Molecules*, vol. 24, no. 16, art. no. 2996, 2019.

[28] M. Humayun, F. Raziq, A. Khan and W. Luo, "Modification strategies

of TiO_2 for potential applications in photocatalysis: a critical review," *Green Chemistry Letters and Reviews*, vol. 11, no. 2, pp. 86–102, 2018.

[29] L. Andronic, D. Perniu and A. Duta, "Synergistic effect between TiO_2 sol–gel and Degussa P25 in dye photodegradation," *Journal of Sol-Gel Science and Technology*, vol. 66, no. 3, pp. 472–480, 2013.